



# A novel design of nanochannel structure in a micro–nanofluidic preconcentrator for electrokinetic ion enrichment

Wenbo Han<sup>1</sup> · Xueye Chen<sup>1</sup>

Received: 14 July 2019 / Accepted: 6 December 2019 / Published online: 16 December 2019  
© The Brazilian Society of Mechanical Sciences and Engineering 2019

## Abstract

Since the concentration of target molecules contained in most reagents in analytical chemistry experiments is lower than the minimum concentration required for subsequent detection, it is necessary for sample enrichment. Electrokinetic trapping that utilizes the principle of ion concentration polarization to achieve biomacromolecular enrichment is the most efficient. In this paper, based on the Poisson–Nernst–Planck equation, a novel design of nanochannel structure in a micro–nanofluidic preconcentrator for electrokinetic ion enrichment is carried out by numerical simulation. The results show that the enrichment process can be divided into three stages: enrichment generation, enrichment promotion and enrichment breakdown when the applied voltage is increased. Importantly, by comparing the six different structure nanochannels (straight line type, square wave type, rectangular type, circle type, zigzag type and multi-wave type), we found that the enrichment ratio produced by the rectangular nanochannel is the highest of the six nanochannels, which is 20.7 times. Rectangular nanochannel requires the lowest applied voltage to achieve the highest enrichment ratio. This work provides a novel design method and theoretical basis for the design of detection equipment in ultra-low concentration molecular detection tasks.

**Keywords** Nanochannel structure · Micro–nanofluidics · Electrokinetic ion enrichment · Ion concentration polarization · Poisson–Nernst–Planck

## 1 Introduction

With the rapid development of micro-nano-manufacturing technology, micro–nanofluidic technology has been widely developed. The functions of preparation, enrichment, separation, purification, mixing, detection and reaction of the sample have been realized on the micro–nanofluidic chips [1–3]. Therefore, miniaturization and personalized analysis experiments are completed on the micro–nanofluidic chip [4, 5]. The main advantages of the micro–nanofluidic chips are small sample consumption, rapid response, low manufacturing cost and so on. So micro–nanofluidic chips have been widely used in life sciences, chemical engineering and environmental engineering [6–10].

Enrichment, separation, purification and detection are involved in the analysis of chemical experiments on micro–nanofluidic chips. The enrichment of the samples is mainly for molecular detection tasks with very low concentration. There are many ways to enrich, such as field amplified sample stacking (FASS) [11], isoelectric focusing (IEF) [12], dielectrophoretic trapping (DEPT) [13, 14] and electrokinetic trapping (EKT) [15–18]. Among them, EKT of enriching charged molecules by using the principle of ion concentration polarization (ICP) is the most efficient [19]. The principle of ICP mainly applies the characteristics of nanochannels for selective transport of ions [20]. As the pioneers of ICP theory, Pu et al. [21] first demonstrated the enrichment and consumption of ions at both ends of a negatively charged glass nanochannel and theoretically explained the ICP phenomenon. Wang et al. [22] used a micro–nanofluidic chip to achieve an enrichment rate of fluorescein isothiocyanate that increased to 600 times in 120 s at 120 V. Jain et al. [23] shown that the sub-2 nm pores separated in graphene are opposite to the larger pores and exhibit different transport behaviors consistent with ion transport under the free energy barrier caused by ion dehydration

---

Technical Editor: Erick de Moraes Franklin, Ph.D.

✉ Xueye Chen  
xueye\_chen@126.com

<sup>1</sup> Faculty of Mechanical Engineering and Automation, Liaoning University of Technology, Jinzhou 121001, China

and electrostatic interaction. Yang et al. [24] found that the voltage-controlled surface charge pattern and ion current rectification are caused by the enhanced cation concentration in the bipolar bilayer and the negatively charged silicon nitride nanopore. Prakash et al. [25] indicated that while maintaining the overall system electrical neutrality, the addition of trace amounts of divalent  $Mg^{2+}$  ions to the nitric oxide (NaCl) electrolyte solution increased the maximum electroosmotic rate of the solution by nearly two times. Through investigating nanopore electrode arrays (NEA) with different geometries, Ma et al. [26] determined the individual contribution of ion accumulation and ion migration to the entire additional current amplification (AFad), achieving a large AFad value in NEA with smaller pores.

Most of the above studies focused on ion transport in straight line nanochannels or nanopores. However, few studies conducted on nanochannels with different structures. In the previous research work, we used numerical simulation to study the ion enrichment of high-viscosity fluids and the Cantor fractal nanochannel. In previous work, we found that the wall structure of nanochannels has a significant impact on electro-nanoparticle enrichment [27, 28]. In view of the important guiding position of electrokinetic ion enrichment theory in ultra-low concentration molecular detection tasks, it is necessary to carry out research on ion transport in different structures of nanochannels.

In this paper, based on the Poisson–Nernst–Planck (PNP) equation, the ion enrichment of six different structure nanochannels in the micro–nanofluidic preconcentrator was studied by numerical simulation. Analysis of the principle of electrokinetic ion enrichment is discussed in detail. The results show that the enrichment process can be divided into three stages. The rectangular type has the highest enrichment rate of 20.7 times. This work provides a novel design for equipment in ultra-low concentration tasks.

## 2 Methodology

We have established a mathematical model and conducted numerical simulation analysis. The numerical simulation of this work is based on the finite element software *COMSOL Multiphysics*<sup>®</sup>. In order to study the nanochannel structure in a micro–nanofluidic preconcentrator for nano-electrokinetic ion enrichment, a set of coupled partial differential equations are solved, including the Poisson equation, the Nernst–Planck equation and the Navier–Stokes equation [29].

**Electric field** The Poisson equation (Eq. 1) is applied to solve the distribution of the electrical potential. The distribution of the electrical potential depends mainly on the applied voltage and surface charge.

$$\nabla \cdot (\epsilon_r \epsilon_0 \nabla \phi) = - \sum_{k=1}^N e z_k n_k \quad (1)$$

In the above equation,  $\epsilon_r$  is relative permittivity,  $\epsilon_0$  denotes electrical permittivity of the vacuum,  $\phi$  represents potential,  $e$  is elementary charge,  $z_k$  is the valence of the  $k$ th ion,  $k$  is the  $k$ th species and  $n_k$  is concentration of the  $k$ th ion.

**Ionic concentration field** As shown in Eq. (2), the Nernst–Planck equation was used to simulate ion transport and ion concentration distribution which depended on the electrophoresis, electroosmosis and diffusion in the micro-nano-composite channel.

$$\frac{\partial n_k}{\partial t} + \nabla \cdot (-w_k z_k n_k \nabla \phi) - \nabla \cdot (D_k \nabla n_k) + \nabla \cdot (n_k u) = 0 \quad (2)$$

where  $u$  is fluid velocity,  $w_k$  and  $D_k$  are electrophoretic mobility and ion diffusion coefficient.

**Flow field** The incompressible Navier–Stokes equation (Eq. 3) with electrical force ( $-\rho_e \nabla \phi$ ) and the continuity equation (Eq. 4) are used to describe the flow field. This means that the density of the fluid is always constant.

$$\rho_0 (\partial_t u + u \cdot \nabla u) = -\nabla p + \mu \nabla^2 u - \rho_e \nabla \phi \quad (3)$$

$$\nabla \cdot u = 0 \quad (4)$$

where  $\rho_0$  is fluid density,  $p$  is pressure,  $\mu$  is dynamic viscosity of fluid and  $\rho_e$  is volumetric charge density.

A two-dimensional numerical model as shown in Fig. 1a is designed. The preconcentrator consists of two microchannels and one nanochannel. The length and width of the microchannels are  $a$  and  $b$ , respectively. The width of the nanochannel is 20 nm. The vertical distance between the two microchannels is 1  $\mu$ m. Then six different nanochannels as shown in Fig. 1b were designed to connect the two microchannels. S1 is a straight line type. S2 is a square wave type. S3 is a rectangular type. S4 is a circle type. S5 is a zigzag type. S6 is a multi-wave type. Their dimensions are shown in Fig. 1b. In this paper, potassium chloride (KCl) can be completely dissociated into  $K^+$  ions and  $Cl^-$  ions in aqueous solution. Detailed ion physical parameters are shown in Table 1. The boundary conditions of the two-dimensional geometric model are shown in Table 2.

## 3 Mesh independence

We use the model of the S1 structure to divide four different numbers of grids to test the grid independence. The number of grids is 8784, 10,724, 11,936 and 15,184. The physical parameters and boundary conditions of the fluid are set as the parameters in Tables 1 and 2. The applied electric

**Fig. 1** The two-dimensional design of the micro–nanofluidic preconcentrator. **a** Two-dimensional geometric model of the preconcentrator with micro-nano-composite channels. **b** Six different structures of nanochannels: (S1) straight line type, (S2) square wave type, (S3) rectangular type, (S4) circle type, (S5) zigzag type, (S6) multi-wave type

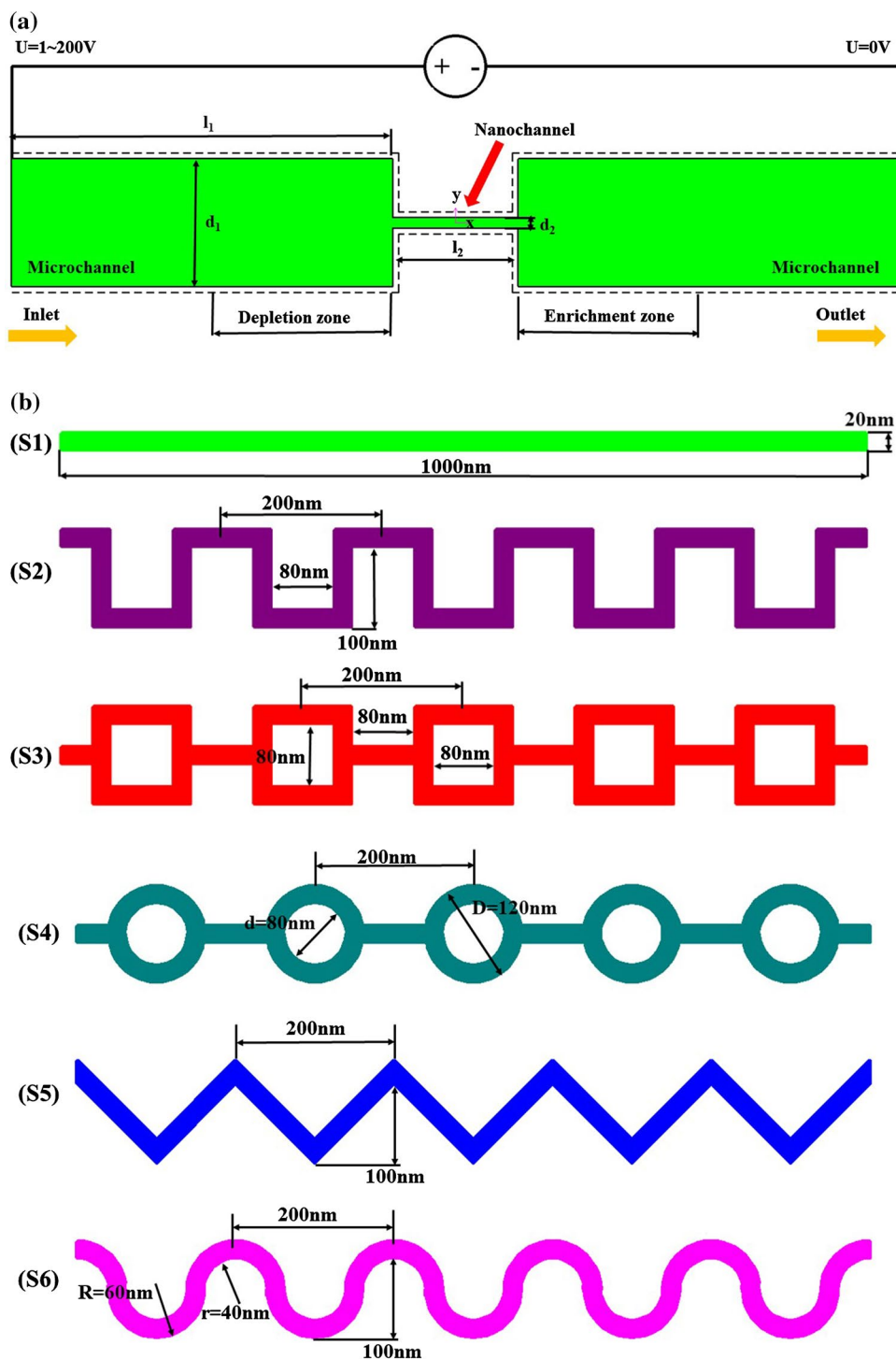


**Table 1** The value of the ion parameter in the simulation

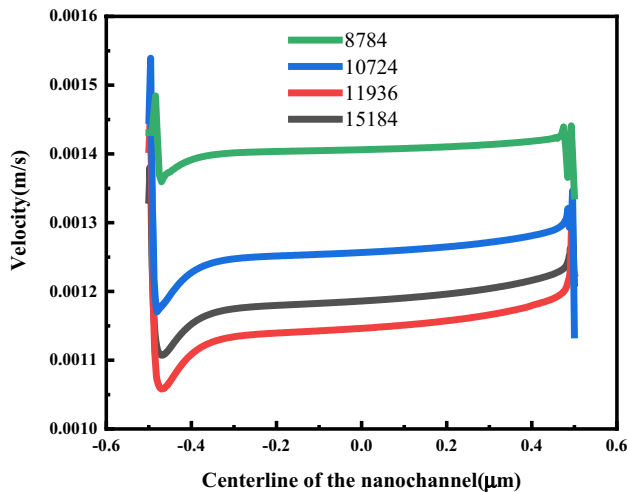
$\rho_0$ (kg/m <sup>3</sup> )	$\epsilon_0$ (F/m)	$\epsilon_r$	$D_1/D_2$ (m <sup>2</sup> /s)	$\mu$ (Pa s)	$z_1/z_2$
$1.0 \times 10^3$	$8.85 \times 10^{-12}$	80	$1.97 \times 10^{-9}/2.01 \times 10^{-9}$	$1.0 \times 10^{-3}$	1/-1

field voltage is fixed at 100 V. We obtained the velocity profile at the centerline of the nanochannel under different grids as shown in Fig. 2. From Fig. 2, it is found that the

velocity value is within the error tolerance range when the number of grids is 11,936. Therefore, in order to reduce the amount of calculation and maintain the accuracy of the

**Table 2** Boundary conditions of the model in the simulation

	Inlet and outlet	The wall of the microchannel	The wall of the nanochannel
Electric field	$\phi_{\text{inlet}} = 1-200 \text{ V}$ , $\phi_{\text{outlet}} = 0 \text{ V}$	$\sigma_{\text{micro}} = -8e^{-4} \text{ C/m}^2$	$\sigma_{\text{nano}} = -8e^{-4} \text{ C/m}^2$
Ionic field	$c_{\text{inlet}} = c_{\text{outlet}} = 0.1 \text{ mol/m}^3$	$j_{\perp} = 0$	$j_{\perp} = 0$
Flow field	$p = 0 \text{ Pa}$	$u = 0$	$u = 0$

**Fig. 2** Velocity at the centerline of the nanochannel under different grids

calculation results, we use a meshing scheme with a grid number 11,936. The mesh in the nanochannel is 5 nm, and the mesh in the microchannel is 50 nm.

## 4 Results and discussion

Ion enrichment through straight line structure nanochannel (S1) was investigated. It can be clearly seen from Fig. 3a that the process of ion enrichment has a peak voltage. The enrichment ratio is gradually increased as the applied voltage is increased. When the applied voltage reaches a peak, the enrichment ratio reaches a maximum value. It can be seen from Fig. 3a that the enrichment ratio is 10.86 and the peak voltage is 56 V. When the applied voltage continues to increase, the enrichment ratio begins to decrease. When the applied voltage is between 56 and 140 V, the enrichment ratio drops rapidly. When the applied voltage is between 140 and 200 V, the enrichment rate decreases at a slower rate. Therefore, the process of ion enrichment can be divided into three stages: enrichment generation, enrichment promotion and enrichment breakdown. To further explain the reasons, the ion concentration image at the applied voltages of 16 V, 36 V, 56 V and 76 V, the concentration curve and the velocity curve on the centerline of the micro-nanochannel were plotted. As can be seen from Fig. 3b–d, when the applied voltage rises from 16 to 36 V, the concentration near the

entrance of the nanochannel decreases. However, the concentration near the exit of the nanochannel increases. This is due to the selective transport properties of the nanochannels. When the applied voltage has not reached the peak voltage, even if the applied voltage is increased, the electrophoretic force generated by the electrophoretic effect is not sufficient to balance the repulsive force generated by the overlap of the electric double layer. The dominant repulsive force causes ions to pass through the nanochannels to the anode region, thus creating an enrichment at the exit of the nanochannel. As the applied voltage increases, the electroosmotic flow in the nanochannels strengthens. Therefore, the flow rate in the nanochannel is increased. When the applied voltage reaches a peak voltage of 56 V, the ion concentration of the enrichment region reaches a peak. The velocity in the nanochannel also reaches the peak velocity. As the applied voltage continues to increase, the ion concentration in the enrichment zone decreases. However, the ion concentration in the depletion region increases. The velocity within the nanochannel decreases. This is because the electrophoretic force is generated by the electrophoretic effect when the applied voltage is increased exceeds the repulsive force generated by the overlap of the electric double layer. Therefore, the ion selective permeability of the nanochannel is broken. The ions reach the anode region through the nanochannel due to the electrophoretic effect.

In order to study the effect of nanochannel structure on ion enrichment, we added the same boundary conditions as S1 on the remaining five nanochannels. The curve of the ion enrichment ratio of the six different structural nanochannels and the concentration image corresponding to the peak voltage were plotted. It can be seen from Fig. 4a that the rates of increase in the ion enrichment ratio of the four channels of S1, S2, S5 and S6 are uniform when the applied voltage is increased. The rates of increase in S2 and S3 ion enrichment ratio are significantly higher than that of the other four structures. This is due to the relatively complicated shunt-convergence structure of S3 and S4. The fluid needs to flow longer in S3 and S4 structures. It is found from Fig. 4a that when the nanochannel has such a complicated structure, the enrichment performance of the nanochannel is enhanced. In order to clearly see the ion concentration distribution at the peak voltage, ion concentration diagrams of the six structures at the peak voltage were obtained, respectively. Figure 4b shows that the S3 structure has a peak voltage of 97 V consistent with the S5 structure. However, the enrichment

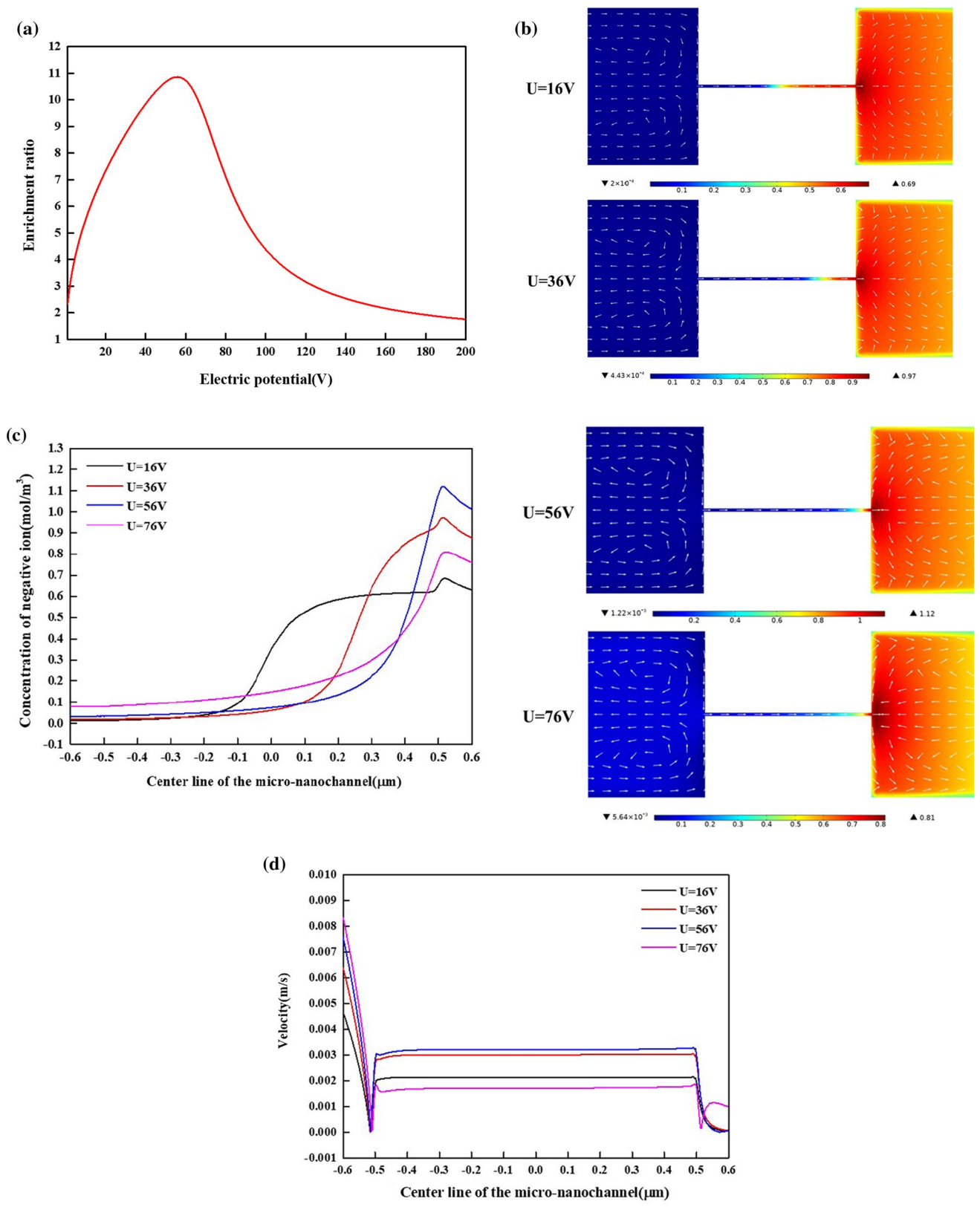
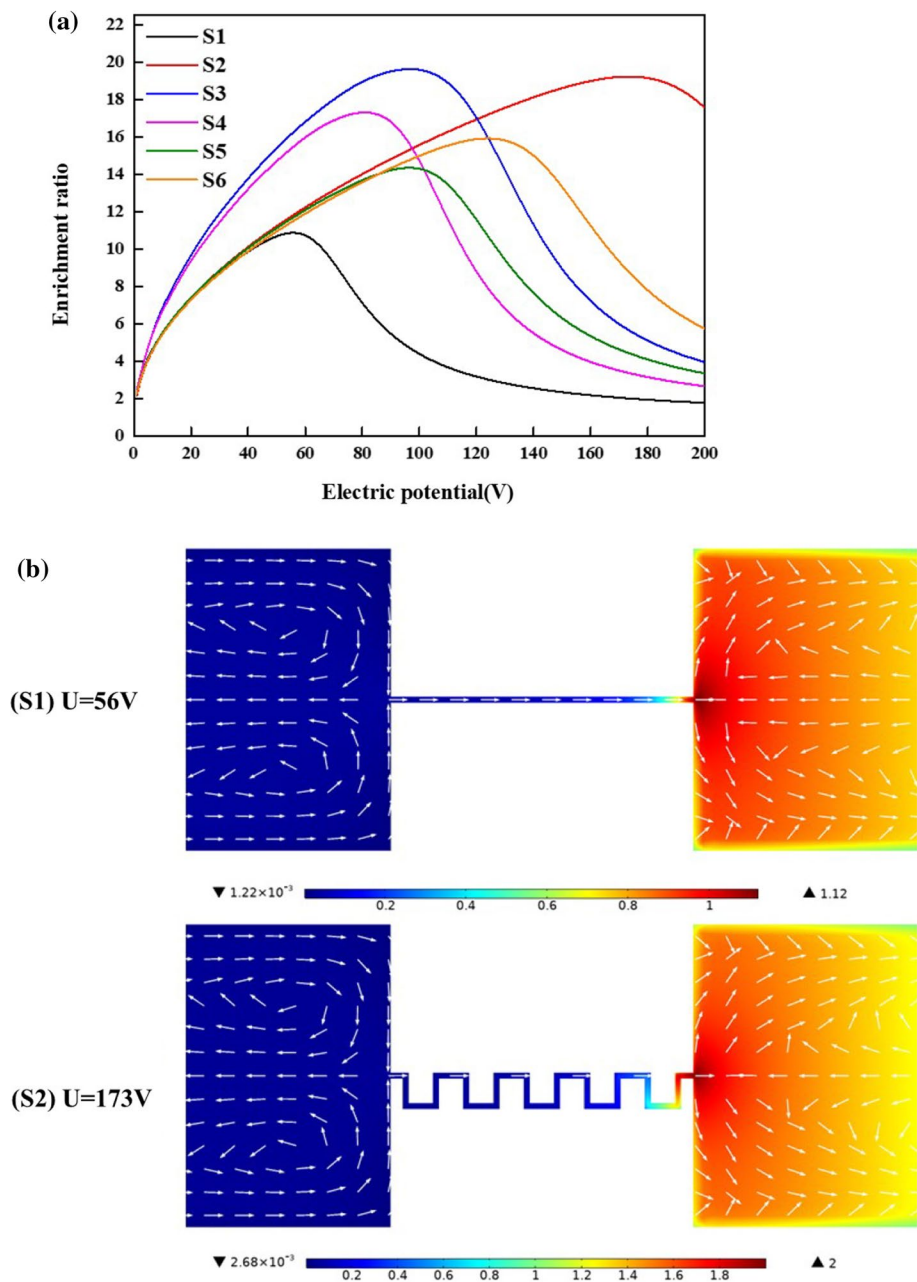


**Fig. 3** a The curve of the enrichment ratio of the straight line type with the applied voltage. b Anion concentration image when applied voltages are 16 V, 36 V, 56 V and 76 V, respectively. c The concentration curve of anions on the centerline of the micro-nano-composite

channel when the applied voltages are 16 V, 36 V, 56 V and 76 V, respectively. d The velocity curve at the centerline of the micro-nano-composite channel when the applied voltages are 16 V, 36 V, 56 V and 76 V

**Fig. 4** **a** The curve of the ion enrichment ratio of the six different structure nanochannels. **b** The concentration image corresponding to the peak voltage for six different structure nanochannels

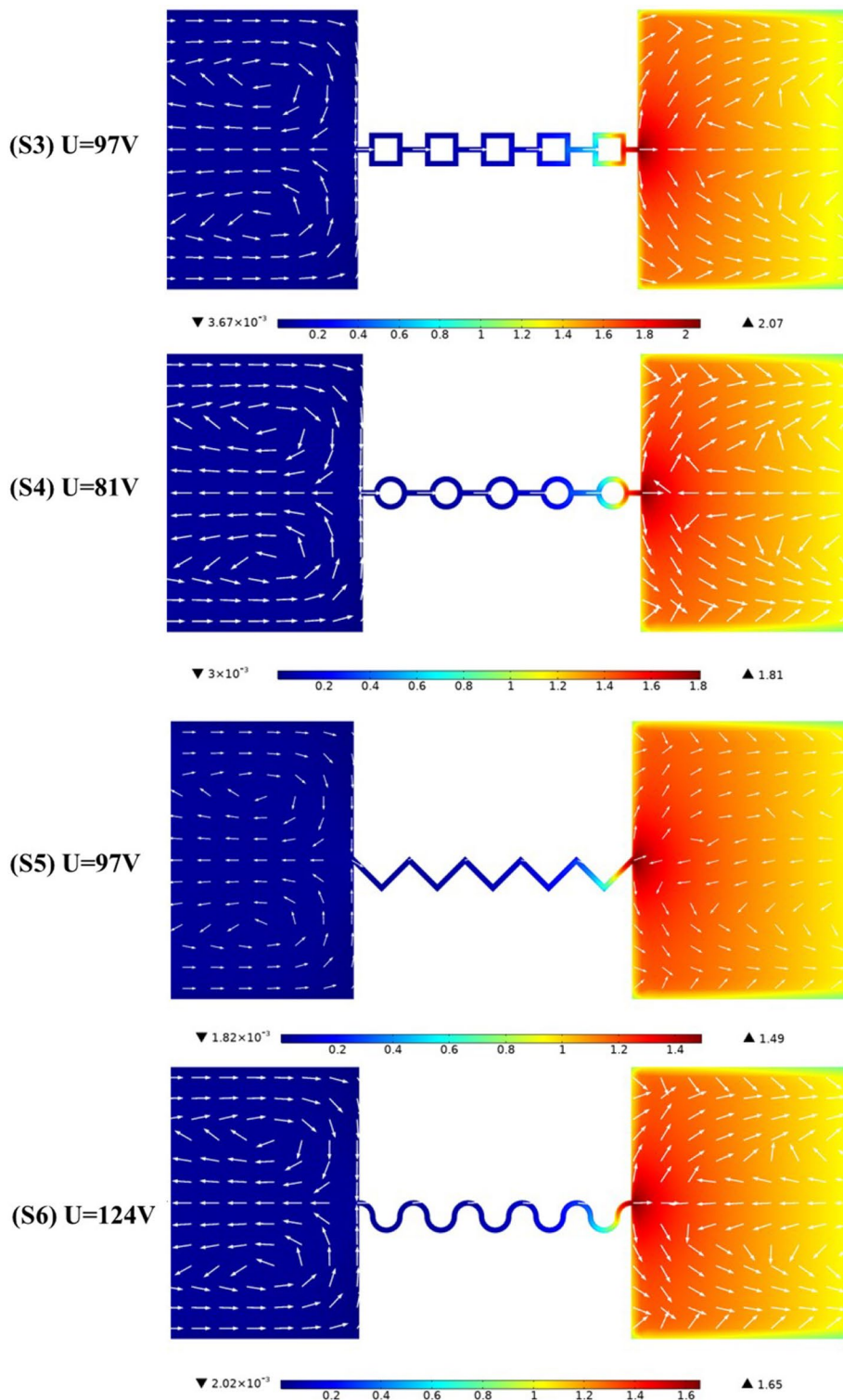


performance of S3 structure is much higher than that of S5. The enrichment ratio of S3 is higher than that of S5 by five times. It can be known from the peak voltages of the six structures that the peak voltage of the nanochannel having the shunt-convergence structure is lower than the peak voltage of the three structures (S2, S5 and S6). In terms of enrichment ratio, the enrichment ratio of S2 and S3 is 20.7 times. However, the applied voltage of S3 is significantly lower than S2. This means that the advantages of the S3 structure are particularly evident in some experiments that require lower voltage. Then, four kinds of S1, S2, S5 and S6 without complex shunt-convergence structure were studied. The study found that their enrichment ratio and peak voltage

are ranked as  $S2 > S6 > S5 > S1$ . It is revealed that anions do not easily pass through such nanochannel due to the presence of a right-angled nanochannel in the S2 structure. Therefore, the S2 structure requires a larger applied voltage to provide a stronger electrophoretic force to overcome this obstacle due to the right-angled nanochannel.

In order to further study the effect of the nanochannels of this shunt-convergence structure on electrokinetic ion enrichment, we have conducted in-depth research on the two confluent structures of S3 and S4. Previous studies have shown that ion flux is mainly composed of electrophoresis flux, electroosmotic flux and diffusion flux [30]. Since the diffusion coefficient of ions is very small, the diffusion flux

Fig. 4 (continued)



is ignored in this paper. The transport forms of the anion and cation in the micro-nanochannel caused by the applied voltage mainly include electrophoresis migration of ions and ion transport caused by fluid electroosmotic flow. The direction of electrophoresis of the anion is from the cathode to the

anode. The electroosmotic flow direction of the fluid is from the anode to the cathode. Because of the opposite ion transport directions caused by electrophoresis and electroosmotic flow, in order to facilitate the comparison of the effects of electrophoresis and electroosmotic flow on ion enrichment,

a relative flux is defined. The relative flux is equal to the value of the electrophoresis flux minus the electroosmotic flux as follows,

$$\Delta EP - EOF = \int_{\Omega} (\omega_k z_k n_k E - un_k) d\Omega \quad (5)$$

In this way, the enrichment magnification can be quantitatively calculated, and the integration region is as shown in Fig. 5a.

As can be seen from Fig. 5b, c, the electrophoresis flux of anions during the ion enrichment process plays a decisive role. The anion's electroosmotic flux is very weak. It can be seen from Fig. 5d, e that the anion relative flux of the rectangular nanochannel is higher than that of the circular structure in the case of the same applied voltage. Therefore, it also explains why the enrichment ratio of the rectangular nanochannel is higher than the enrichment ratio of the circular nanochannel when the applied voltage is the same.

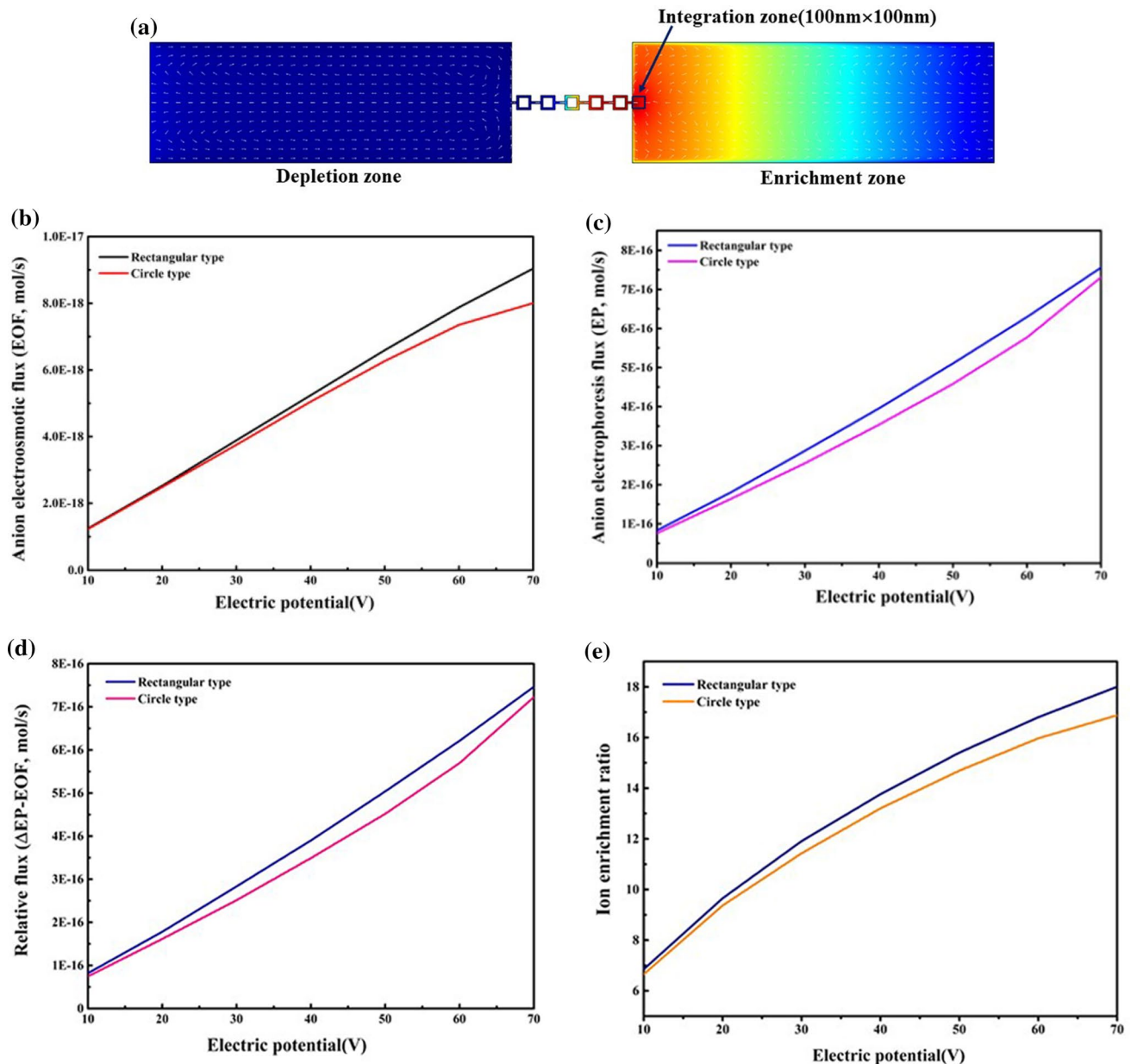


**Fig. 5** a Schematic diagram of the integration zone, b electroosmotic flux of anions in circle and rectangular nanochannels, c electrophoresis flux of anions in circle and rectangular nanochannels, d relative

flux ( $\Delta EP - EOF$ ) of anions in circle and rectangular nanochannels, e ion enrichment ratio in circle and rectangular nanochannels



## 5 Conclusion

In this paper, the ion enrichment of six different structure nanochannels in the micro–nanofluidic preconcentrator was studied by numerical simulation. The results show that with the increase in applied voltage, ion enrichment can be divided into three stages: enrichment generation, enrichment promotion and enrichment breakdown. In addition, the study found that when the applied voltage is the same, the enrichment ratio of the rectangular nanochannel is the highest among the six structural species. Rectangular channels have a maximum enrichment rate of up to 20.7 times. The research results in this paper lay a theoretical foundation for the design of detection equipment in ultra-low concentration molecular detection tasks.

**Acknowledgements** This work was supported by Liaoning Natural Science Foundation (2019-MS-169), the Key Project of Department of Education of Liaoning Province (JZL201715401) and Liaoning BaiQianWan Talents Program. We sincerely thank Prof. Chong Liu for his kind guidance.

## Compliance with ethical standards

**Conflict of interest** The authors declare no conflict of interest.

## References

- Han W, Chen X, Hu Z, Yang K (2018) Three-dimensional numerical simulation of a droplet generation in a double T-junction microchannel. *J Micro/Nanolithogr MEMS MOEMS* 17(2):025502
- Han W, Chen X (2019) Numerical simulation of the droplet formation in a T-junction microchannel by a level-set method. *Aust J Chem* 71(12):957–964
- Han W, Chen X (2019) New insights into the pressure during the merged droplet formation in the squeezing time. *Chem Eng Res Des* 145:213–225
- Zhang S, Chen X (2019) Secondary bonding of PMMA micro-mixer with high-pressure. *Microchem J* 144:339–344
- Zhang S, Chen X, Wu Z, Zheng Y (2019) Numerical study on stagger Koch fractal baffles micromixer. *Int J Heat Mass Transf* 133:1065–1073
- Wang X, Zhu C, Fu T, Ma Y (2014) Critical lengths for the transition of bubble breakup in microfluidic T-junctions. *Chem Eng Sci* 111:244–254
- Timung S, Chaudhuri J, Borthakur MP, Mandal TK, Biswas G, Bandyopadhyay D (2017) Electric field mediated spraying of miniaturized droplets inside microchannel. *Electrophoresis* 38(11):1450–1457
- Santra S, Das S, Das SS, Chakraborty S (2018) Surfactant-induced retardation in lateral migration of droplets in a microfluidic confinement. *Microfluid Nanofluid* 22(8):88
- Anna SL, Bontoux N, Stone HA (2003) Formation of dispersions using “flow focusing” in microchannels. *Appl Phys Lett* 82(3):364–366
- Kim SH, Kim JW, Kim DH, Han SH, Weitz DA (2013) Enhanced-throughput production of polymersomes using a parallelized capillary microfluidic device. *Microfluid Nanofluid* 14(3–4):509–514
- Burgi DS, Chien RL (1991) Optimization in sample stacking for high-performance capillary electrophoresis. *Anal Chem* 63(18):2042–2047
- Cui H, Horiuchi K, Dutta P, Ivory CF (2005) Multistage iso-electric focusing in a polymeric microfluidic chip. *Anal Chem* 77(24):7878–7886
- Gebauer P, Boček P (2000) Recent progress in capillary isotachopheresis. *Electrophoresis Int J* 21(18):3898–3904
- Asbury CL, Van Den Engh G (1998) Trapping of DNA in nonuniform oscillating electric fields. *Biophys J* 74(2):1024–1030
- Kim SJ, Ko SH, Kang KH, Han J (2010) Direct seawater desalination by ion concentration polarization. *Nat Nanotechnol* 5(4):297
- Yeh LH, Zhang M, Hu N, Joo SW, Qian S, Hsu JP (2012) Electrokinetic ion and fluid transport in nanopores functionalized by polyelectrolyte brushes. *Nanoscale* 4(16):5169–5177
- Choi E, Kwon K, Lee SJ, Kim D, Park J (2015) Non-equilibrium electrokinetic micromixer with 3D nanochannel networks. *Lab Chip* 15(8):1794–1798
- Gong L, Ouyang W, Li Z, Han J (2018) Direct numerical simulation of continuous lithium extraction from high  $Mg^{2+}/Li^{+}$  ratio brines using microfluidic channels with ion concentration polarization. *J Membr Sci* 556:34–41
- MacDonald BD, Gong MM, Zhang P, Sinton D (2014) Out-of-plane ion concentration polarization for scalable water desalination. *Lab Chip* 14(4):681–685
- Li M, Anand RK (2016) Recent advancements in ion concentration polarization. *Analyst* 141(12):3496–3510
- Pu Q, Yun J, Temkin H, Liu S (2004) Ion-enrichment and ion-depletion effect of nanochannel structures. *Nano Lett* 4(6):1099–1103
- Wang JY, Xu Z, Li YK, Liu C, Liu JS, Chen L, Du L, Wang LD (2013) Nanopore density effect of polyacrylamide gel plug on electrokinetic ion enrichment in a micro-nanofluidic chip. *Appl Phys Lett* 103(4):043103
- Jain T, Rasera BC, Guerrero RJS, Boutilier MS, O’hern SC, Idrobo JC, Karnik R (2015) Heterogeneous sub-continuum ionic transport in statistically isolated graphene nanopores. *Nat Nanotechnol* 10(12):1053
- Yang C, Hinkle P, Menestrina J, Vlasiouk IV, Siwy ZS (2016) Polarization of gold in nanopores leads to ion current rectification. *J Phys Chem Lett* 7(20):4152–4158
- Prakash S, Zambrano HA, Rangharajan KK, Rosenthal-Kim E, Vasquez N, Conlisk AT (2016) Electrokinetic transport of monovalent and divalent cations in silica nanochannels. *Microfluid Nanofluid* 20(1):8
- Ma C, Xu W, Wichert WR, Bohn PW (2016) Ion accumulation and migration effects on redox cycling in nanopore electrode arrays at low ionic strength. *ACS Nano* 10(3):3658–3664
- Han W, Chen X (2019) Nano-electrokinetic ion enrichment in a micro-nanofluidic preconcentrator with nanochannel’s Cantor fractal wall structure. *Appl Nanosci*. <https://doi.org/10.1007/s13204-019-01049-7>
- Han W, Chen X (2019) Nano-electrokinetic ion enrichment of highly viscous fluids in micro-nanochannel. *Chem Eng Process Process Intensif* 143:107626
- Wang Y, Pant K, Chen Z, Wang G, Diffey WF, Ashley P, Sundaram S (2009) Numerical analysis of electrokinetic transport in micro-nanofluidic interconnect preconcentrator in hydrodynamic flow. *Microfluid Nanofluid* 7(5):683
- Wang J, Liu C, Xu Z (2016) Electrokinetic ion transport in confined micro-nanochannel. *Electrophoresis* 37(5–6):769–774

**Publisher’s Note** Springer Nature remains neutral with regard to jurisdictional claims in published maps and institutional affiliations.